Structural Characterization and Oxidative Dehydrogenation Activity of $V_2O_5/Ce_xZr_{1-x}O_2/SiO_2$ Catalysts

Benjaram M. Reddy,*,† Pandian Lakshmanan,† Stéphane Loridant,‡ Yusuke Yamada,§ Tetsuhiko Kobayashi,§ Carlos López-Cartes,|| Teresa C. Rojas,|| and Asunción Fernández||

Inorganic and Physical Chemistry Division, Indian Institute of Chemical Technology, Hyderabad 500 007, India, Institut de Recherches sur la Catalyze, CNRS, 2 Avenue Albert Einstein, 69626 Villeurbanne Cedex, France, National Institute of Advanced Industrial Science and Technology (AIST), 1-8-31 Midorigaoka, Ikeda, Osaka, 563-8577, Japan, and Instituto de Ciencia de Materiales de Sevilla (CSIC-UNSE), Avenida Américo Vespucio Number 49, 41092 Sevilla, Spain

Received: February 17, 2006; In Final Form: March 20, 2006

The thermal stability of a nanosized $Ce_xZr_{1-x}O_2$ solid solution on a silica surface and the dispersion behavior of V_2O_5 over $Ce_xZr_{1-x}O_2/SiO_2$ have been investigated using XRD, Raman spectroscopy, XPS, HREM, and BET surface area techniques. Oxidative dehydrogenation of ethylbenzene to styrene was performed as a test reaction to assess the usefulness of the $VO_x/Ce_xZr_{1-x}O_2/SiO_2$ catalyst. $Ce_xZr_{1-x}O_2/SiO_2$ (1:1:2 mol ratio based on oxides) was synthesized through a soft-chemical route from ultrahigh dilute solutions by adopting a deposition coprecipitation technique. A theoretical monolayer equivalent to 10 wt % V_2O_5 was impregnated over the calcined $Ce_xZr_{1-x}O_2/SiO_2$ sample (773 K) by an aqueous wet impregnation technique. The prepared $V_2O_5/Ce_xZr_{1-x}O_2/SiO_2$ sample was subjected to thermal treatments from 773 to 1073 K. The XRD measurements indicate the presence of cubic $Ce_{0.75}Zr_{0.25}O_2$ in the case of $Ce_xZr_{1-x}O_2/SiO_2$, while cubic $Ce_{0.5}Zr_{0.5}O_2$ and tetragonal $Ce_{0.16}Zr_{0.84}O_2$ in the case of $V_2O_5/Ce_xZr_{1-x}O_2/SiO_2$ when calcined at various temperatures. Dispersed vanadium oxide induces more incorporation of zirconium into the ceria lattice, thereby decreasing its lattice size and also accelerating the crystallization of Ce−Zr−O solid solutions at higher calcination temperatures. Further, it interacts selectively with the ceria portion of the composite oxide to form $CeVO_4$. The RS measurements provide good evidence about the dispersed form of vanadium oxide and the $CeVO_4$ compound. The HREM studies show the presence of small Ce-Zr-oxide particles of ∼5 nm size over the surface of amorphous silica and corroborate with the results obtained from other techniques. The catalytic activity studies reveal the ability of vanadium oxide supported on $Ce_xZr_{1-x}O_2/SiO_2$ to efficiently catalyze the ODH of ethylbenzene at normal atmospheric pressure. The remarkable ability of $Ce_xZr_{1-x}O_2$ to prevent the deactivation of supported vanadium oxide leading to stable activity in the time-on-stream experiments and high selectivity to styrene are other important observations.

Introduction

Apart from automotive exhaust purification three-way catalytic (TWC) applications, $Ce_xZr_{1-x}O_2$ solid solutions have emerged as powerful combinations in heterogeneous catalysis for various purposes.[1−12] The addition of zirconium to the cubic structure of ceria increases the oxygen storage capacity (OSC) of the system while enhancing its thermal stability as compared to pure ceria; hence, they were exploited in the formulation of the modern TWC catalysts.[1−3] The $Ce_xZr_{1-x}O_2$ combination has also gained much attention as a fascinating catalyst support for noble metals and metal oxides to design various other catalysts for industrially important processes such as oxidation (partial oxidation, total oxidation, preferential oxidation, and combustion),[4−7] reforming/hydrogen production,[8] dehydration,[9] deNO_x,[10] and oxygen sensing applications.[11] This combination has also been proved to be effective in the direct conversion of methane to synthesis gas.[12] The excellent redox property of the $Ce_xZr_{1-x}O_2$ composite oxide can promote the activity of supported metals, while the oxygen transport capability can improve the activity of the metal oxides supported on it.[13] It has been proved experimentally that the oxygen mobility of $Ce_xZr_{1-x}O_2$ influences greatly the catalytic activity of supported transition metal oxides such as CuO (preferential oxidation of CO in hydrogen rich steam reformates), Co_3O_4 and PdO (methane combustion), and NiO (steam reforming of ethanol to generate hydrogen for fuel cell applications).[8,14−16]

Despite the wide applicability of Ce-Zr-oxide solid solutions, the fall of specific surface area, poor structural stability, and mechanical strength due to sintering at high temperatures restricted the use of unsupported forms of Ce-Zr-oxides.[17,18] Numerous methodologies could be found in the literature to synthesize the unsupported forms of $Ce_xZr_{1-x}O_2$.[1] Coprecipitation can lead to a high specific surface area; however, the temperature stability of as-prepared oxides is characterized by a severe loss of surface area at elevated temperatures.[17,18] Flame methods and sol−gel routes require expensive precursors, such as alkoxides.[19,20] Combusting mixtures of redox compounds (urea) and oxidizing metal precursors (nitrates) pose explosion hazards leading to great difficulties in the batch processes.[21]

* Corresponding author. E-mail: bmreddy@iict.res.in or mreddyb@yahoo.com.
† Indian Institute of Chemical Technology.
‡ Institut de Recherches sur la Catalyze.
§ National Institute of Advanced Industrial Science and Technology.
|| Instituto de Ciencia de Materiales de Sevilla.

10.1021/jp061018k CCC: $33.50
Published on Web 04/19/2006

Therefore, there is an ongoing effort to devise an appropriate preparation methodology to disperse nanocomposites of $Ce_xZr_{1-x}O_2$ over a stable inert support for various catalytic applications.

Supported vanadia systems are complex oxides exhibiting interesting catalytic properties that depend on a variety of factors including preparation method, thermal treatment, and nature of support.[22] It has been reported in the literature that V_2O_5/ZrO_2 catalysts exhibit a high activity for certain oxidative dehydrogenations, selective catalytic reduction of NO_x, and other reactions.[23−26] The V_2O_5/CeO_2 combination catalysts have also been reported to display good catalytic properties for oxidative conversion of propane to propylene and ethane to ethylene, preferential oxidation of CO to CO_2, and other reactions.[27−32] Therefore, the unique combination of excellent redox features of $Ce_xZr_{1-x}O_2$ and the oxidizing ability of the dispersed vanadium oxide is expected to result in a good catalytic system with numerous application prospects. The present investigation was undertaken against the aforementioned background. In this study, a nanosized $Ce_xZr_{1-x}O_2$ solid solution highly dispersed on a SiO_2 support was synthesized through a soft-chemical route by adopting a deposition coprecipitation method. A theoretical monolayer equivalent of V_2O_5 (10 wt %) was deposited over a calcined $Ce_xZr_{1-x}O_2/SiO_2$ support (773 K) by a wet impregnation method. The prepared $V_2O_5/Ce_xZr_{1-x}O_2/SiO_2$ catalyst was subjected to thermal treatments from 773 to 1073 K to understand the dispersion and temperature stability of the catalyst. The structural evolution was investigated by using XRD, Raman spectroscopy, XPS, HREM, and BET surface area methods. The catalytic performance was evaluated for oxidative dehydrogenation (ODH) of ethylbenzene to styrene in the vapor phase at normal atmospheric pressure. Styrene is an important monomer extensively used in the polymer industry for the manufacture of polymers, copolymers, and reinforced plastics. Styrene is normally produced by two methods: as a coproduct of propylene oxide production and by dehydrogenation (DH) of ethylbenzene catalyzed by potassium-promoted iron oxides.[33] The ODH of ethylbenzene is a third possibility to produce styrene, which has gained much attention recently. The advantage of the ODH process is that, unlike the endothermic dehydrogenation processes, it can be operated at a lower temperature, as it is exothermic.

Experimental Procedures

Catalyst Preparation. The $Ce_xZr_{1-x}O_2/SiO_2$ (CZS) composite oxide (1:1:2 mol ratio based on oxides) was prepared by a deposition coprecipitation method. In a typical experiment, requisite quantities of ammonium cerium(IV) nitrate (Loba Chemie, GR grade) and zirconium(IV) nitrate (Fluka, AR grade) were dissolved separately in deionized water and mixed together. The required quantity of colloidal silica (Ludox 40 wt %, Aldrich, AR grade) was added to the aforementioned mixture solution. Dilute aqueous ammonia was added dropwise with vigorous stirring until the precipitation was complete (pH = 8.5). The resulting product was filtered off, washed several times with deionized water, oven dried at 383 K for 12 h, and then calcined at 773 K for 5 h in air atmosphere. The $V_2O_5/Ce_xZr_{1-x}O_2/SiO_2$ (VCZS) sample with a nominal 10 wt % V_2O_5 was prepared by a standard wet impregnation method. To impregnate V_2O_5, the required quantity of ammonium metavanadate (Fluka, AR grade) was dissolved in an aqueous oxalic acid solution (1 M). To this clear solution, the finely powdered calcined (773 K) $Ce_xZr_{1-x}O_2/SiO_2$ support was added. The excess water was evaporated using a water bath, and the resulting material was oven dried at 393 K for 12 h and subsequently calcined at 773 K for 5 h in a closed electrical furnace in an oxygen atmosphere. Some portions of the finished catalyst were once again heated at 873, 973, and 1073 K for 5 h in air atmosphere.

Catalyst Characterization. The X-ray powder diffraction (XRD) patterns were acquired with a Siemens D-5005 diffractometer using Ni-filtered Cu K_α radiation. Matching experimental patterns with the PDF-ICDD, the XRD phases were identified. The mean crystallite size was measured by applying the Scherrer equation. The Raman spectra were recorded by using a DILOR XY Raman spectrometer equipped with a liquid-nitrogen cooled charge-coupled device (CCD) detector. Raman excitation at 514.5 nm was provided by an Ar^+ laser (Spectra Physics) that was focused on the sample under the microscope, the width of the analyzed spot being ~1 μm. A laser power of 3 mW at the sample was typically applied, and the time of acquisition was adjusted according to the intensity of the Raman scattering. The wavenumbers reported are within to 2 cm^{-1}.

The XPS measurements were performed on a Shimadzu (ESCA 3400) spectrometer by using Mg K_α (1253.6 eV) radiation as the excitation source. Charging of catalyst samples was corrected by setting the binding energy of the adventitious carbon (C 1s) at 284.6 eV. The XPS analysis was done at ambient temperature and pressures typically below 10^{-6} Pa. The HREM investigations were performed using a Philips CM200 electron microscope with a 0.23 nm point-to-point resolution. The samples were supported on a holey carbon grid by dropping ethanol suspensions containing uniformly dispersed oxide powers. The BET surface area measurements were made using a Gemini 2360 instrument by N_2 physisorption at liquid nitrogen temperature. Prior to analysis, samples were degassed at 393 K under vacuum for 8 h to remove the adsorbed moisture and other volatiles.

Catalytic Activity. The catalytic activity for vapor phase ODH of ethylbenzene was investigated in a down flow fixed-bed microreactor at different temperatures under normal atmospheric pressure. In a typical experiment, ca. 0.5 g of the sample was secured between two plugs of Pyrex glass wool inside the glass reactor (Pyrex glass tube, o.d. 1 cm and i.d. 0.8 cm) and above the catalyst bed filled with glass chips to act as a preheating zone. The reactor was placed vertically inside a tubular furnace, which could be heated electrically and connected to a temperature indicator-controller. The catalyst was preactivated in a flow of air at 723 K for 5 h prior to the reaction. After the activation, the temperature was adjusted to the desired level, and ethylbenzene was fed from a motorized syringe pump (Perfusor Secura FT, Germany) into the vaporizer where it was allowed to mix uniformly with dry air before entering the preheating zone of the reactor. The liquid products collected through spiral condensers in the ice cooled freezing traps were analyzed by a gas chromatograph with flame ionization detector. The main products obtained were styrene, benzene, and toluene along with some traces of unidentified products. The activity data were collected under steady-state conditions. The conversion and selectivity were calculated as per procedures described elsewhere.[34]

Results and Discussion

High specific surface area is one of the most important requirements for mixed oxides for various catalytic applications. The surface area, particle size, and resistance to thermal sintering of $Ce_xZr_{1-x}O_2$ are reported to be strongly dependent on the synthetic methodology.[1] Generally, ultrafine particles exhibit a

TABLE 1: BET Surface Area and Crystallite Size Measurements of $Ce_xZr_{1-x}O_2/SiO_2$ (CZS) and 10% $V_2O_5/Ce_xZr_{1-x}O_2/SiO_2$ (VCZS) Samples Calcined at Different Temperatures

sample/calcinations temperature (K)	surface area (m^2/g)	crystallite size[a] (nm)
	CZS	
773	172	3.1
	VCZS	
773	102	3.3
873	88	4.75
973	74	n.d.[b]
1073	55	n.d.

[a] From most prominent XRD. [b] n.d.: not determined due to compositional heterogeneity.

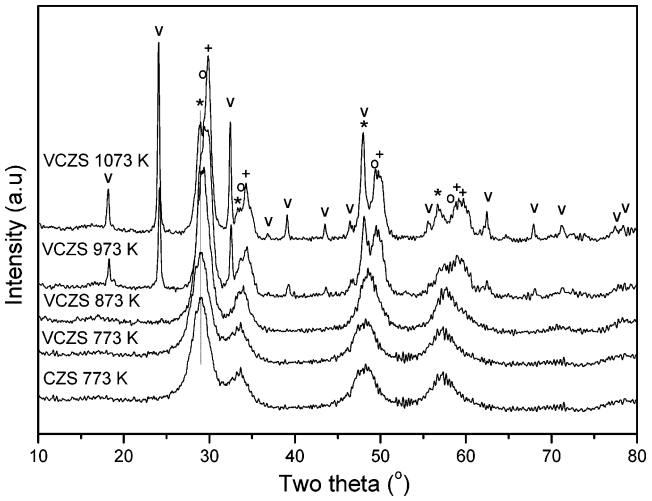

Figure 1. X-ray diffraction patterns of $Ce_xZr_{1-x}O_2/SiO_2$ (CZS) calcined at 773 K and 10% $V_2O_5/Ce_xZr_{1-x}O_2/SiO_2$ (VCZS) calcined at different temperatures. Peak legends are as follows: (*) lines due to $Ce_{0.75}Zr_{0.25}O_2$, (○) lines due to $Ce_{0.5}Zr_{0.5}O_2$, (+) lines due to $Ce_{0.16}Zr_{0.84}O_2$, and (v) lines due to $CeVO_4$.

very high specific surface area because of their smaller sizes. To achieve a high surface area of $Ce_xZr_{1-x}O_2$ solid solutions with a small particle size and good thermal resistance, colloidal silica was used as an inert stabilizer in the present investigation. The specific surface area and particle size measurements of the resulting samples are presented in Table 1. As can be noted from this table, the CZS sample exhibits a BET surface area of 172 $m^2\ g^{-1}$ and below a 5 nm crystallite size. The vanadia loaded sample (VCZS) calcined at 773 K exhibited a surface area of 102 $m^2\ g^{-1}$, which showed a ~50% decrease upon increasing the calcination temperature from 773 to 1073 K. The decrease in the surface area of the V_2O_5 impregnated sample (773 K) with respect to pure support is due to the penetration of the dispersed vanadium oxide into the pores of the support, thereby narrowing its pore diameter.[34] The substantial decrease in the surface area at higher calcination temperatures is due to sintering and solid-state reactions between the dispersed vanadium oxide and the support as evidenced by other characterization techniques discussed in the subsequent paragraphs. Nevertheless, the VCZS sample retains a high specific surface area with a smaller particle size even after calcination at higher temperatures (Table 1).

The X-ray powder diffraction patterns of CZS and VCZS samples calcined at 773 and 773−1073 K, respectively, are presented in Figure 1. In general, the XRD patterns typically feature broad diffraction lines due to nanometric dimension of the crystallites. A cubic fluorite type phase with a composition $Ce_{0.75}Zr_{0.25}O_2$ (PDF-ICDD 28-0271) could be identified from the diffraction patterns of the CZS sample calcined at 773 K. The vanadia loaded VCZS sample calcined at 773 K exhibits an almost similar diffraction pattern of the CZS, and the vanadia features are clearly absent. This observation indicates that the dispersed vanadium oxide is in an amorphous state. This fact is supported by RS measurements described in the later paragraphs. Both a gain in intensity of the peaks and a progressive upward shift in the peak positions of the XRD patterns could be noted with increasing calcination temperature beyond 873 K. The observed shifts in the 2θ values are mainly due to a gradual increase of zirconium content into the ceria unit cell (for eight-coordinated M^{4+}, $r_{Zr4+} = 0.84$ Å and $r_{Ce4+} = 0.97$ Å).[1] The substitution of smaller zirconium ions into the ceria structure induces a contraction of the unit cell volume and hence the shortening of the lattice distance. Consequently, the occurrence of cubic $Ce_{0.5}Zr_{0.5}O_2$ (PDF-ICDD 38-1436) and tetragonal zirconium rich $Ce_{0.16}Zr_{0.84}O_2$ (PDF-ICDD 38-1437) phases are manifested from the XRD patterns of the VCZS sample calcined at 1073 K. Additional sharp peaks are also observed at 973 K due to the formation of the $CeVO_4$ (PDF-ICDD 12-0757) compound. The intensity of these lines increased with an increasing calcination temperature due to better crystallization. It appears from these results that impregnated vanadium oxide under the influence of thermal treatments accelerates the crystallite growth, induces more incorporation of zirconium into the ceria lattice, and also leads to the formation of $CeVO_4$ by selective interaction with the cerium cations of the $Ce_xZr_{1-x}O_2/SiO_2$ sample. According to Kenevey et al.,[35] the phase segregation phenomenon is surface energy driven and depends on the particle size. The increase in calcination temperature increases the crystallite size accelerated by the dispersed vanadia and a subsequent fall of contribution to the total surface energy of the system where it is stabilized. The XRD investigations further provide interesting information that there are no compounds between various component oxides (CeO_2, SiO_2, ZrO_2, and V_2O_5) of the sample such as $Ce_{9.33}(SiO_4)_6O_2$, $ZrSiO_4$, and ZrV_2O_7, except $CeVO_4$, as reported in the literature.[36,37] This could be attributed to various factors such as a strong interaction between the cerium and the zirconium oxides to form solid solutions, the use of an inert colloidal silica as a support, and lower calcination temperatures employed in the present study.

A selective interaction of the dispersed vanadium oxide with one of the component oxides of a mixed oxide system appears to be very interesting.[38,39] In the case of V_2O_5/TiO_2-SiO_2 catalysts, the impregnated vanadium oxide selectively interacts with the titania portion of the mixed oxide and forms a $V_xTi_{1-x}O_2$ rutile solid solution when subjected to more than a 773 K calcination temperature.[38,39] However, in the case of V_2O_5/ZrO_2-TiO_2 samples, a preferential interaction of V_2O_5 with ZrO_2 to form ZrV_2O_7 at 773 K and above has been observed.[38] Interestingly, in the case of VCZS, the deposited vanadium oxide interacts selectively with the cerium cations of the composite oxide to form $CeVO_4$. This kind of selective interaction of vanadia with one of the components of the mixed oxides could be related to the ratio of charge on the support cation to the sum of the radii of the cation and oxide ions.[39] A smaller ratio favors compound formation in general, and this ratio becomes larger for Zr(IV) because of the smaller ionic radii of Zr(IV), as compared to that of Ce(IV).[40] Within the detection limits of the XRD technique, there is no evidence for the presence of *t*-ZrO_2 or *m*-ZrO_2 phases. Additionally, the XRD features of silica are also not apparent, indicating the amorphous nature of the support. Clearly, the absence of silica features in the XRD

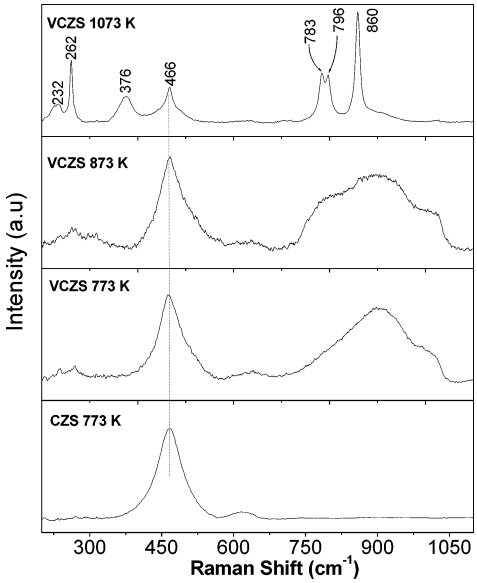

Figure 2. Raman spectra of $Ce_xZr_{1-x}O_2/SiO_2$ (CZS) and $V_2O_5/Ce_xZr_{1-x}O_2/SiO_2$ (VCZS) samples calcined at different temperatures.

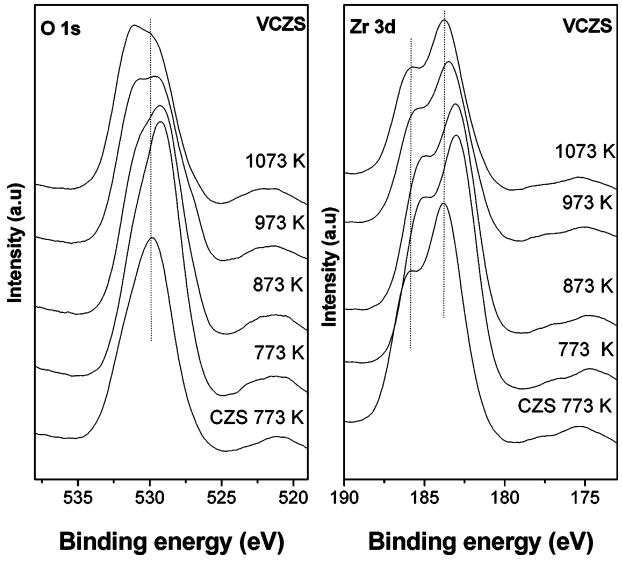

Figure 3. O 1s and Zr 3d XPS spectra of $Ce_xZr_{1-x}O_2/SiO_2$ (CZS) and $V_2O_5/Ce_xZr_{1-x}O_2/SiO_2$ (VCZS) samples calcined at different temperatures.

profiles of both CZS and VCZS samples calcined at 1073 K may be taken as an indication of the coverage of the silica surface with the component oxides.

In contrast to the cation-dominated information provided by the XRD technique, Raman spectra of fluorite structure related phases are dominated by the lattice oxygen vibrations, which are sensitive to the crystal symmetry, being thus a potential tool to obtain additional structural information.[41] The Raman spectra of CZS and VCZS samples calcined at 773 and 773−1073 K, respectively, are depicted in Figure 2. The CZS sample calcined at 773 K exhibits a broad and intense Raman band at 466 cm^{-1} and a weak and broad feature at ∼620 cm^{-1}. The main peak at 466 cm^{-1} is due to a F_{2g} Raman active mode typical of fluorite structured material.[42] The broad and weak band observed at ∼620 cm^{-1} could be attributed to a nondegenerate Raman inactive LO mode of cerium oxide. The appearance of this band is due to the presence of the oxygen vacancy concentration, which perturbs the local M−O bond symmetry leading to the relaxation of symmetry selection rules.[43] It should be mentioned here that this band is observed due to the nanosized nature of the Ce-Zr-oxides in which the amount of defect sites is expected to be more.

The VCZS sample calcined at 773 K exhibited a broad band in the range of 740−1040 cm^{-1}, a sharp band at 465 cm^{-1}, and a weak feature at ∼237 cm^{-1}. The sharp band observed at 465 cm^{-1} was due to the F_{2g} vibration mode of the cubic type ceria lattice of the *Fm*3*m* space group, as mentioned earlier.[42] The broad bands in the range of 740−1040 cm^{-1} correspond to the presence of hydrated polyvanadate species.[44,45] This broad feature disappeared, and new bands appeared at 262, 376, 783, 796, and 860 cm^{-1} upon calcination at 973 and 1073 K. These new bands are due to the formation of a $CeVO_4$ compound, which is in agreement with XRD results.[46,47] The intensity of these bands increased with an increase of calcination temperature from 973 to 1073 K at the expense of the bands due to the fluorite type ceria lattice. At 873 K, additional broad bands are observed at around 260, 780, and 860 cm^{-1}, indicating the nucleation of a new phase. These bands could be due to $CeVO_4$ nanocrystallites. Silica did not show any Raman features, as reported in the literature, probably due to the coverage of its surface by the deposited oxides.[48] If formed, the ZrV_2O_7 phase could be identified by the presence of intense bands at ∼770 and 985 cm^{-1}.[24] Also, the crystalline V_2O_5 exhibits Raman bands at 990, 701, 528, 407, 303, and 283 cm^{-1}.[49] From Raman spectra of VCZS samples, there is no indication of the presence of these oxides. Furthermore, no specific Raman bands pertaining to other compounds such as $Ce_{9.33}(SiO_4)O_2$ and $ZrSiO_4$ as reported in the literature are apparent. The absence of these features is mainly due to a different preparation method adopted and lower calcination temperatures employed in the present investigation. The Raman results thus corroborate well with the XRD data.

TABLE 2: XPS Core Level Binding Energies (eV) of $Ce_xZr_{1-x}O_2/SiO_2$ (CZS) and 10% $V_2O_5/Ce_xZr_{1-x}O_2/SiO_2$ (VCZS) Samples Calcined at Different Temperatures

	binding energy (eV)				
temperature (K)	O 1s	Zr 3d	Ce 3d	Si 2p	V 2p
		CZS			
773	530.2	183.7	881.7	102.9	
		VCZS			
773	529.6	183.0	881.5	102.4	517.8
873	529.7	183.1	881.5	102.8	517.4
973	529.8−531.3	183.4	881.4	103.1	517.5
1073	530.0−531.8	183.7	881.3	103.4	517.8

To understand the nature of electronic interactions between various oxides, the CZS and VCZS samples were subjected to XPS analysis, and the corresponding electron binding energies (eV) of O 1s, Zr 3d, Si 2p, Ce 3d, and V 2p are presented in Table 2. Figure 3 displays the O 1s and Zr 3d XPS spectra of CZS sample calcined at 773 K and the VCZS sample calcined at 773−1073 K. In general, the O 1s profile is very broad owing to the overlapping contributions from silica and ceria-zirconia solid solutions in the case of pure support and silica, ceria-zirconia solid solutions, and dispersed vanadium oxide in the case of vanadia impregnated samples. The observed binding energy at 530.2 eV from the center of the symmetric curve for the CZS sample could be attributed to the O 1s ionization of oxygen associated with the $Ce_{0.75}Zr_{0.25}O_2$ solid solution.[50,51] The emergence of $CeVO_4$ upon high temperature calcination accompanied by the formation of zirconium rich $Ce_xZr_{1-x}O_2$ solid solutions with different compositions could be the reason for the observed changes in the binding energy and broadening of the peaks in the case of VCZS samples, which are slightly different from that of the CZS sample. Bifurcation and broaden-

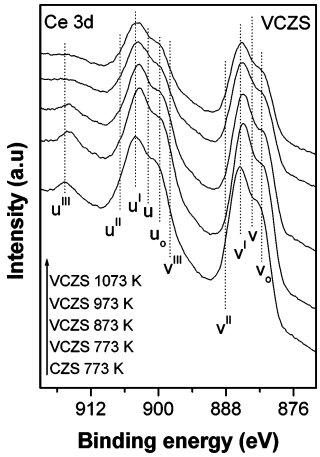

Figure 4. Ce 3d XPS spectra of $Ce_xZr_{1-x}O_2/SiO_2$ (CZS) and $V_2O_5/Ce_xZr_{1-x}O_2/SiO_2$ (VCZS) samples calcined at different temperatures.

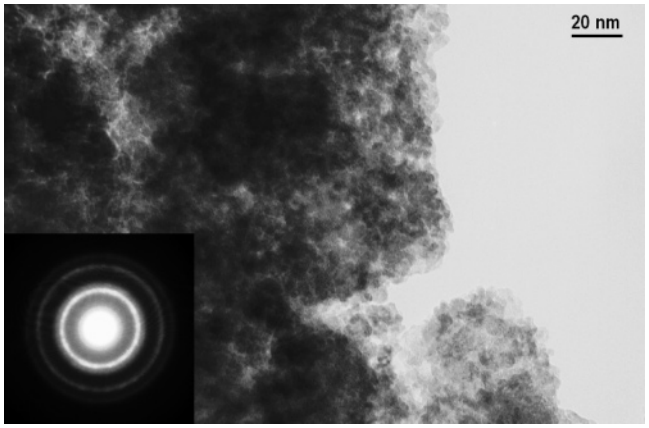

Figure 5. TEM image of $Ce_xZr_{1-x}O_2/SiO_2$ (CZS) sample calcined at 773 K. The inset in the image is the digital diffraction pattern (DDP) obtained from the corresponding image.

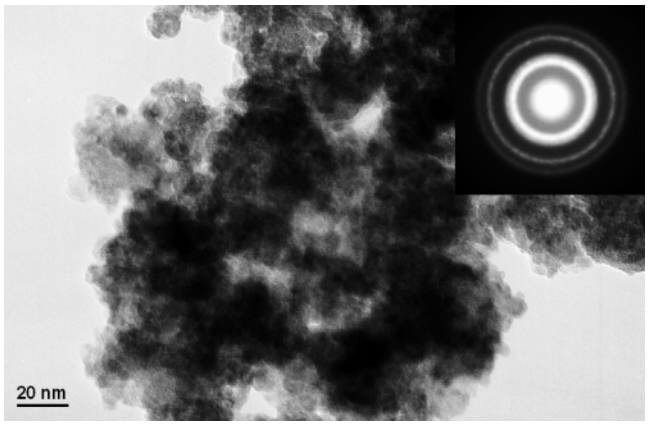

Figure 6. TEM image of 10% $V_2O_5/Ce_xZr_{1-x}O_2/SiO_2$ (VCZS) sample calcined at 773 K. The inset in the image is the digital diffraction pattern (DDP) obtained from the corresponding image.

ing of the peaks are clearly noted at 973 and 1073 K due to the $CeVO_4$ formation as established from XRD and Raman measurements. As shown in Table 2, the binding energy of the Zr 3d photoelectron peak ranged between 183.0 and 183.7 eV, which agrees well with the values reported in the literature.[51,52] As presented in Figure 3, the core level spectra of Zr 3d in the case of the VCZS samples is slightly different from that of CZS sample, which exhibit a progressive broadening along with small binding energy shifts with increasing calcination temperatures. These observed changes could be due to the formation of zirconium rich $Ce_xZr_{1-x}O_2$ solid solutions and $CeVO_4$ under the influence dispersed vanadium oxide as pointed out earlier. In particular, the observed binding energy of Zr 3d in the range of 183.3−183.7 eV could be taken as evidence for the absence of ZrO_2 since a binding energy value of 182.9 eV is expected for ZrO_2.[53]

The binding energy of the Si 2p photoelectron peaks ranged between 102.4 and 103.4 eV for various samples in this study, which agree well with the values reported in the literature.[50,51] However, the poor intensity of the spectra with large peak widths indicated that SiO_2 is not easily accessible at the surface due to the presence of Ce-Zr-oxides, vanadium oxide, and cerium vanadate overlayers. The presence of oxidized silicon has been abundantly described in the literature, sometimes as CeO_{2-x}/SiO_2[54,55] or as an amorphous silicate layer,[56,57] where partial reduction of Ce(IV) to Ce(III) occurs together with partial oxidation of Si. The formation of either $CeSiO_4$ or $ZrSiO_4$ could be identified by the Si 2p binding energy value of 101 eV,[58] and clearly these are absent. The V 2p binding energy values ranged between 517.4 and 517.8 eV in good agreement with the literature reports[59,60] and correspond to a V^{5+} oxidation state. As can be noted from Table 2, there is a slight shift in the binding energy values upon increasing the calcination temperature from 773 to 1073 K. Broadening of the V 2p peak was also observed with an increasing calcination temperature (not shown). These observations give an impression that initially some V^{5+} cations could be reduced to lower oxidation states due to an increased calcination temperature and formation of $CeVO_4$ and broaden further during successive calcination treatments at 973 and 1073 K.

The complexity of the Ce 3d photoelectron spectra is well-known and has been rationalized in terms of a hybridization between the partially occupied 4f levels of the Ce and 2p states of oxygen.[61] The Ce 3d spectra pertaining to various samples has been presented in Figure 4 and analyzed following the labeling first used by Burroughs et al.;[62] the peaks labeled v correspond to Ce $3d_{5/2}$ contributions, and those of labeled u represent the Ce $3d_{3/2}$ contributions. Specifically, the bands u_o and u are due to Ce $3d_{3/2}$ ionization, and bands v_o and v are Ce $3d_{5/2}$ ionizations for Ce^{3+} and Ce^{4+}, respectively. The bands labeled v′, v″, and v‴ are satellites arising from the $3d_{5/2}$ ionization, while the bands u′, u″, and u‴ represent Ce $3d_{3/2}$ ionization. The spectra pertaining to the CZS sample indicate the presence of both Ce(III) and Ce(IV) oxidation states, in accordance with the literature reports that Ce becomes easily reducible due to the formation of solid solutions with zirconia. Such reduction was found to be at a maximum when the composition was $Ce_{0.5}Zr_{0.5}O_2$.[63] The u‴ peak is the most convenient feature to follow the progressive Ce reduction since it does not overlap with others. It can be noticed from Figure 4 that the intensity of the u‴ peak decreases upon increasing the calcination temperature for VCZS samples. This could be related to the emergence of the $CeVO_4$ phase upon increasing the calcination temperature and can be attributed to the remarkable ability of the surface vanadia to remove the most easily reducible surface oxygen of CeO_2 and facile formation of $CeVO_4$ phase by readily switching between Ce(IV) and Ce(III).[31] Thus, XPS measurements provide interesting information on the structural evolution of these samples.

The TEM images along with selected area electron diffraction patterns (SAED) of CZS and VCZS samples calcined at 773 K are shown in Figures 5 and 6, respectively. These and other images (not shown) clearly reveal similar features, in line with XRD observations, with the existence of small particles (∼5

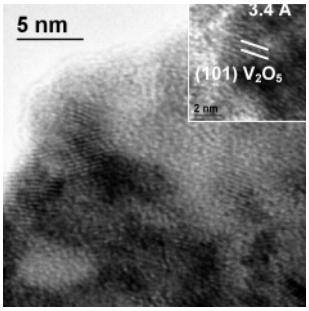

Figure 7. HREM image of $V_2O_5/Ce_xZr_{1-x}O_2/SiO_2$ (VCZS) sample calcined at 773 K. The periodicity of 3.4 Å corresponds to the (101) plane of the V_2O_5 crystal structure.

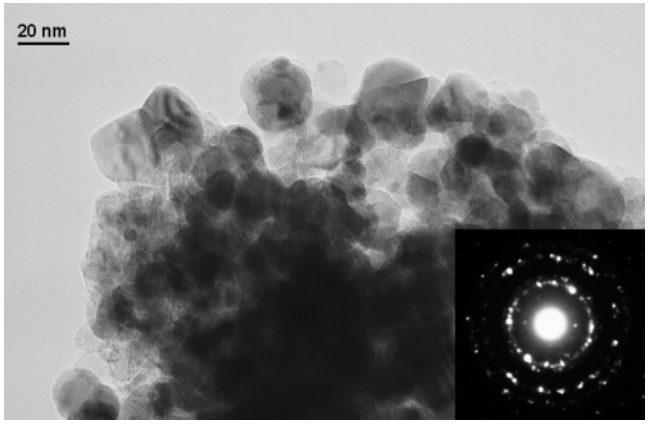

Figure 8. TEM image of VCZS sample calcined at 1073 K. The inset in the image is the digital diffraction pattern (DDP) obtained from the corresponding image.

nm) dispersed over an amorphous matrix with different lighter contrasts. The position of the reflections in the electron diffraction pattern and broadening of the rings indicate the presence of small randomly oriented Ce-Zr mixed oxide particles with an almost exclusively cubic structure. The detection of highly dispersed vanadium oxide on oxide supports is difficult from the TEM technique. The dispersed vanadium oxide will be present mostly in the form of small amorphous aggregates on the surface of the support, which could be hardly seen if the texture of the support is complicated like the present one. However, some contrasts observed in the experimental HREM images of the VCZS sample calcined at 773 K reveal its identity as shown in Figure 7. As can be noted, in addition to the Ce-Zr oxide phases, small particles showing lattice fringes with a periodicity of 3.4 Å are detected as are the resultant *d* spacings corresponding to the (101) plane of the V_2O_5 structure. The TEM global picture of the VCZS sample calcined 1073 K is shown in Figure 8. Well-distinguished single spots conform the rings in the SAED pattern and reveal an increase of particle size due to sintering during high temperature calcination. The appearance of some extra spots, closer to the center of the diagram, is associated to larger *d* spacings and could be attributed to the formation of new phases during heat treatment in the presence of vanadium oxide. The HREM image of the corresponding specimen is presented in Figure 9, which reveals two different types of crystal structures. The lattice fringes of around 3 Å are extensively observed on very small particles supported on an amorphous contrast of silica, which denote the $Ce_xZr_{1-x}O_2$ solid solution particles. Periodicities of 3.7 Å could be detected, which can be attributed to the (200) planes of the $CeVO_4$ phase, which is clearly identified from XRD and Raman results. Thus, the TEM results corroborate well with the observations made from XRD and RS measurements.

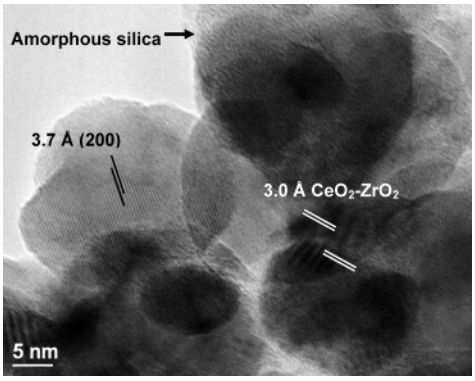

Figure 9. HREM image of 10% $V_2O_5/Ce_xZr_{1-x}O_2/SiO_2$ (VCZS) sample calcined at 1073 K. The periodicity of 3.0 Å corresponds to a $Ce_xZr_{1-x}O_2$ solid solution, and 3.7 Å corresponds to $CeVO_4$.

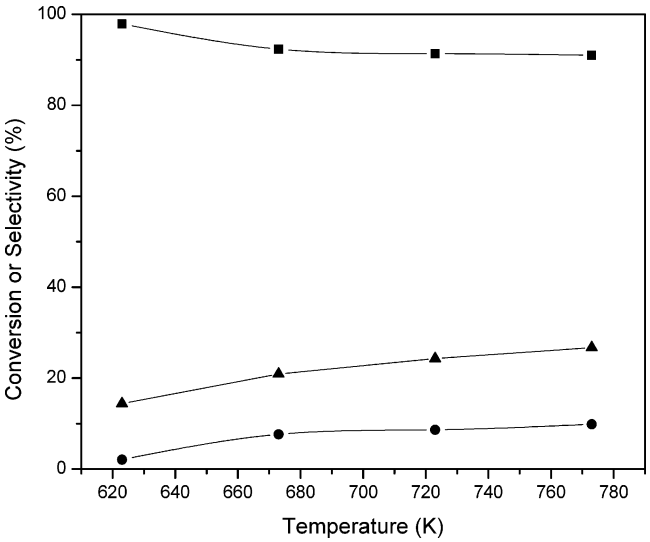

Figure 10. Effect of temperature on conversion and product selectivity over 10% $V_2O_5/Ce_xZr_{1-x}O_2/SiO_2$ (VCZS) sample. (▲) Ethylbenzene conversion, (■) styrene selectivity, and (●) sum of the selectivities of side products (benzene and toluene).

Supported vanadium oxide catalysts are known to catalyze the oxidative dehydrogenation of alkanes with a high activity and selectivity. Interestingly, the oxidant used in the ODH reaction plays a crucial role in determining the selectivity of the desired product and the stability of the catalytic action of the vanadia species. The use of O_2, CO_2, SO_2, N_2, dry air, and N_2O gases as oxidants has been investigated for the ODH processes. The application of O_2 and SO_2 leads to deep oxidation of ethylbenzene to CO_x and the formation of toxic side products, respectively.[64] CO_2 as an oxidant results in the formation of carbonaceous deposits resulting in fast deactivation of the catalyst, and N_2O leads to more styrene oxide selectivity.[65] On the other hand, the use of pure N_2 suffers from the problem of unavailability of oxygen resulting in low product yields. In view of these reasons, in the present investigation, the ODH of ethylbenzene was carried out using dry air as the oxidant. The reaction was performed at an ethylbenzene space velocity of 1 h^{-1} and a dry air space velocity of 1600 h^{-1}. The reaction was carried out at various temperatures while keeping all other parameters constant to investigate the effect of temperature on the conversion and selectivity. Figure 10 represents the effect of temperature on the conversion of ethylbenzene, selectivity of styrene, and other products over a $V_2O_5/Ce_xZr_{1-x}O_2/SiO_2$ catalyst calcined at 773 K. As can be noted from this figure, the conversion of ethylbenzene and the selectivity to dealkylate

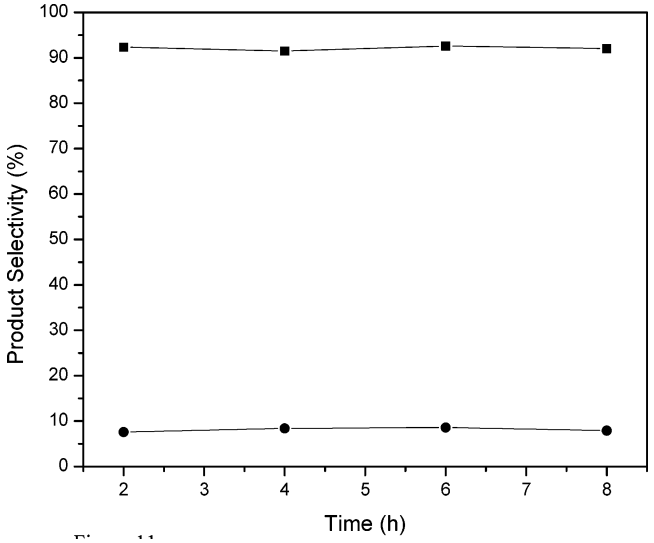

Figure 11. Product selectivities as a function of time-on-stream over 10% $V_2O_5/Ce_xZr_{1-x}O_2/SiO_2$ (VCZS) sample. Reaction temperature 673 K, (■) styrene selectivity, and (●) sum of the selectivities of side products (benzene and toluene).

side products (benzene and toluene together) increases with an increasing reaction temperature as expected. The selectivity to styrene is appreciable and quite stable with marginal decreases at high reaction temperatures. Interestingly, under identical conditions, the $Ce_xZr_{1-x}O_2/SiO_2$ support alone was found to show only dealkylation side products, which clearly signifies the role of vanadium oxide in ODH reactions. The time-on-stream experiments reveal an interesting catalytic behavior of the VCZS sample toward the ODH of ethylbenzene, as shown in Figure 11. As can be noted from this figure, the selectivity of styrene in the time-on-stream experiments resulted into a straight line within the investigated time limits, indicating a quite stable activity. The sum of the selectivities of dealkylation side products is also found to remain less and does not show an appreciable increase with time-on-stream. These results reveal a good catalytic efficiency of V_2O_5 without deactivation when supported on $Ce_xZr_{1-x}O_2/SiO_2$.[65] A fast deactivation is noted in most of the cases during time-on-stream experiments on different catalyst systems.[65] Recent literature reports reveal that ceria-zirconia mixed oxide supports can produce a stable catalytic activity during time-on-stream runs. The NiO_x/Ce-Zr-oxide catalyst exhibited a stable activity for syn-gas production via CO_2 reforming methane without a significant loss during the reaction for 100 h.[66] Similar trends were noticed for partial oxidation of methane (POM),[67] dehydration of 4-methyl-2-pentanol,[9] and methane combustion.[68] On the contrary, a rapid deactivation was noticed in the case of the VO_x/Al_2O_3 catalyst.[65] The stable activity was attributed to the facile oxygen transport from the bulk of $Ce_xZr_{1-x}O_2$ solid solutions that helps in the prevention of coke formation, which is the main deactivation pathway of these catalysts. Thus, the obtained stable activity for the ODH of ethylbenzene in the present study is in good agreement with the literature reports. The remarkable ability of $Ce_xZr_{1-x}O_2/SiO_2$ to stabilize the catalytic activity of dispersed vanadia is clearly apparent in the present study.

Conclusions

(1) A theoretical monolayer equivalent to 10 wt % V_2O_5 was impregnated on the $Ce_xZr_{1-x}O_2/SiO_2$ mixed oxide synthesized by a deposition coprecipitation technique. The obtained $VO_x/Ce_xZr_{1-x}O_2/SiO_2$ was subjected to various thermal treatments from 773 to 1073 K to examine the dispersion and structural stability of the catalyst. (2) The physicochemical characteristics and crystalline structure of $Ce_xZr_{1-x}O_2$ solid solutions are strongly influenced by the dispersed vanadium oxide and thermal treatments. (3) The XRD results revealed the presence of $Ce_{0.75}Zr_{0.25}O_2$ in the case of the $Ce_xZr_{1-x}O_2/SiO_2$ sample calcined at 773 K, while $Ce_{0.5}Zr_{0.5}O_2$ and $Ce_{0.16}Zr_{0.84}O_2$ were observed in the case of the $VO_x/Ce_xZr_{1-x}O_2/SiO_2$ sample calcined beyond 873 K. (4) Raman spectroscopy measurements revealed highly dispersed vanadium oxide on $Ce_xZr_{1-x}O_2/SiO_2$ at 773 K and the formation of $CeVO_4$ at higher calcination temperatures. (5) The HREM results confirmed a well-dispersed nanosized $Ce_xZr_{1-x}O_2$ solid solution (<5 nm) over the surface of amorphous silica with an exclusively cubic structure in the case of the $Ce_xZr_{1-x}O_2/SiO_2$ sample calcined at 773 K. Also, the formation of $CeVO_4$ at higher calcination temperatures was confirmed in the case of the $V_2O_5/Ce_xZr_{1-x}O_2/SiO_2$ sample. (6) The catalytic activity study for ODH of ethybenzene revealed the ability of $Ce_xZr_{1-x}O_2/SiO_2$ to prevent deactivation of the catalyst, providing a stable activity with good styrene product selectivity during the time-on-stream experiments.

Acknowledgment. P.L. thanks CSIR, New Delhi for a Senior Research Fellowship. C.L.-C. thanks the I3P program (CSIC) for a postdoctoral contract. Financial support was received from the Department of Science and Technology, New Delhi under a SERC Scheme (SR/S1/PC-31/2004).

References and Notes

(1) Di Monte, R.; Kaspar, J. *J. Mater. Chem.* **2005**, *15*, 633 and references therein.
(2) Velasco, J. R. G.; Ortiz, M. A. G.; Marc, J. L.; Botas, J. A.; Marcos, M. P. G.; Blanchard, G. *Appl. Catal., B* **1999**, *22*, 167.
(3) Yao, H. C.; Yu Yao, Y. F. *J. Catal.* **1984**, *86*, 254.
(4) Passos, F. B.; de Oliveira, E. R.; Mattos, L. V.; Noronha, F. B. *Catal. Today* **2005**, *101*, 23.
(5) Gélin, P.; Primet, M. *Appl. Catal., B* **2002,** *39*, 1.
(6) Mariño, F.; Descorme, C.; Duprez, D. *Appl. Catal., B* **2005**, *58*, 175.
(7) Ciuparu, D.; Pfefferle, L. *Appl. Catal., A* **2001**, *218*, 197.
(8) Srinivas, D.; Satyanarayana, C. V. V.; Potdar, H. S.; Ratnasamy, P. *Appl. Catal., A* **2003**, *246*, 323.
(9) Solinas, V.; Rombi, E.; Ferino, I.; Cutrufello, M. G.; Colón, G.; Navío, J. A. *J. Mol. Catal.* **2003**, *205*, 629.
(10) Chen, F.; González, G.; Wang, J. A.; Noreña, L. E.; Toledo, A.; Castillo S.; Pineda, M. M. *Appl. Surf. Sci.* **2005**, *243*, 319.
(11) Izu, N.; Hori, N. O.; Itou, M.; Shin, W.; Matsubara, I.; Murayama, N. *Sens. Actuators, B* **2005**, *108*, 238.
(12) Otsuka, K.; Wang, Y.; Nakamura, M. *Appl. Catal., A* **1999**, *183*, 317.
(13) Ciuparu, D.; Pfefferle, L. *Catal. Today* **2002**, *77*, 167.
(14) Ratnasamy, P.; Srinivas, D.; Satyanarayana, C. V. V.; Manikandan, P.; Senthil Kumaran, R. S.; Sachin, M.; Shetti, V. N. *J. Catal.* **2004**, *221*, 455.
(15) Liotta, L. F.; Di Carlo, G.; Pantaleo, G.; Deganello, G. *Catal. Commun.* **2005**, *6*, 329.
(16) Dragos, C.; Perkins, E. E.; Pfefferle, L. *Appl. Catal., A* **2004**, *263*, 145.
(17) Bozo, C.; Gaillard, F.; Guilhaume, N. *Appl. Catal., A* **2001**, *220*, 69.
(18) Si, R.; Zhang, Y.-W.; Li, S.-J.; Lin, B.-X.; Yan, C.-H. *J. Phys. Chem. B* **2004**, *108*, 12481.
(19) Laine, R. M.; Bickmore, C. R.; Waldner, K. F. U.S. Patent 5,614,-596, 1995.
(20) Gutsch, A.; Henning, T.; Katusic, S.; Krämer, M.; Michael, G.; Varga, G. J. European Patent 1,142,830 A1, 2000.
(21) Aruna, S. T.; Patil, K. C. *Nanostruct. Mater.* **1998**, *10*, 955.
(22) Adamski, A.; Sojka, Z.; Dyrek, K.; Che, M.; Wendt, G.; Albrecht, S. *Langmuir* **1999**, *15*, 5733 and references therein.
(23) Khodakov, A.; Yang, J.; Su, S.; Iglesia, E.; Bell, A. T. *J. Catal.* **1998**, *177*, 343.
(24) Male, J. L.; Niessen, H. G.; Bell, A. T.; Don Tilley, T. *J. Catal.* **2000**, *194*, 431.

(25) Christodoulakis, A.; Machli, M.; Lemonidou, A. A.; Boghosian, S. *J. Catal*, **2004**, *222*, 293.
(26) Szakacs, S.; Altena, G. J.; Fransen, T.; Van Ommen J. G.; Ross, J. R. H. *Catal. Today* **1993**, *16*, 237.
(27) Daniell, W.; Ponchel, A.; Kuba, S.; Anderle, F.; Weingand, T.; Gregory, D. H.; Knözinger, H. *Top. Catal*. **2002**, *20*, 65.
(28) Rane, V. H.; Rajput, A. M.; Karkamkar, A. J.; Choudhary, V. R. *Appl. Energy* **2004**, *77*, 375.
(29) Feng, T.; Vohs, J. M. *J. Catal*. **2004**, *221*, 619.
(30) Burcham, L. J.; Deo, G.; Gao, X.; Wachs, I. E. *Top. Catal*. **2000**, *11*, 85.
(31) Martinez-Huerta, M. V.; Coronado, J. M.; Fernandez-Garcia, M.; Iglesias-Juez, A.; Deo, G.; Fierro, J. L. G.; Banares, M. A. *J. Catal*. **2004**, *225*, 240.
(32) Wootsch, A.; Descorme, C.; Duprez, D. *J. Catal*. **2004**, *225*, 259.
(33) Cavani, F.; Trifirò, F. *Appl. Catal., A* **1995**, *133*, 219.
(34) Reddy, B. M.; Kumar, M. V.; Ratnam, K. J. *Appl. Catal., A* **1999**, *181*, 77.
(35) Kenevey, K.; Valdivieso, F.; Soustelle, M.; Pijolat, M. *Appl. Catal., B* **2001**, *29*, 93.
(36) Rocchini, E.; Trovarelli, A.; Liorca, J.; Graham, G. W.; Weber, W. H.; Maciejewski, M.; Baiker, A. *J. Catal*. **2000**, *194*, 461.
(37) Kucharczyk, B.; Tylus, W.; Kepinski, L. *Appl. Catal., B* **2004**, *49*, 27.
(38) Reddy, B. M.; Chowdhary, B.; Ganesh, I.; Reddy, E. P.; Rojas, T. C.; Fernández, A. *J. Phys. Chem. B* **1998**, *102*, 10176.
(39) Bond, G. C.; Tahir, S. F. *Appl. Catal.* **1991**, *71*, 1 and references therein.
(40) Pengpanich, S.; Meeyoo, V.; Rirksomboon, T.; Bunyakiat, K. *Appl. Catal., A* **2002**, *234*, 221.
(41) Knözinger, H.; Mestl, G. *Top. Catal.* **1999**, *8*, 45.
(42) Lin, X.-M.; Li, L.-P.; Li, G.-S.; Su, W.-H. *Mater. Chem. Phys.* **2001**, *69*, 236.
(43) Weber, W. H.; Hass, K. C.; McBride, J. R. *Phys. Rev. B* **1993**, *48*, 178.
(44) Roozeboom, F.; Hazelger, M. C. M.; Moulijn, J. A.; de Beer, J.; Gellings, P. J. *J. Phys. Chem.* **1980**, *84*, 2783.
(45) Reddy, B. M.; Lakshmanan, P.; Khan, A.; Lopez-Cartes, C.; Rojas, T. C.; Fernandez, A. *J. Phys. Chem. B* **2005**, *109*, 1781.
(46) Hirata, T.; Watanabe, A. *J. Solid State Chem.* **2001**, *158*, 254.
(47) Reddy, B. M.; Khan, A. *Catal. Surv. Jpn.* **2005**, *9*, 155.
(48) Wachs, I. E.; Deo, G. *J. Phys. Chem*. **1991**, *95*, 5889.
(49) Banares, M. A.; Wachs, I. E. *J. Raman Spectrosc.* **2002**, *33*, 359.
(50) Wagner, C. D.; Riggs, W. M.; Davis, L. E.; Moulder, J. F. In *Handbook of X-ray Photoelectron Spectroscopy*; Muilenberg, G. E., Ed.; Perkin-Elmer Corporation: Eden Prairie, MN, 1978.
(51) Briggs, D.; Seah, M. P. *Auger and X- ray Photoelectron Spectroscopy, Practical Surface Analysis*, 2nd ed.; Wiley: New York, 1990; Vol. 1.
(52) Reddy, B. M.; Khan, A.; Yamada, Y.; Kobayashi, T.; Loridant, S.; Volta, J.-C. *Langmuir* **2003**, *19*, 3025.
(53) Wong, P. C.; Li, Y. S.; Mitchell, K. A. R. *Surf. Rev. Lett*. **1995**, *2*, 297.
(54) Galtayries, A.; Crucifix, M.; Blanchard, G.; Terwagne, G.; Sporken, R. *Appl. Surf. Sci*. **1999**, *142*, 159.
(55) Nagata, H.; Yoshimoto, M.; Tsukahara, T.; Gonda, S.; Koinuma, H. *Mater. Res. Soc. Symp. Proc.* **1991**, *202*, 445.
(56) Inoue, T.; Yamamoto, Y.; Satoh, M.; Ide, A.; Katsumata, S. *Thin Solid Films* **1996**, *281*, 24.
(57) Sanchez, F.; Varela, M.; Ferrater, C.; Cuenca, M. V. G.; Aguiar, R.; Morenza, J. L. *Appl. Surf. Sci*. **1993**, *70*, 94.
(58) Behner, H.; Wecker, J.; Mathee, T.; Samwer, K. *Surf. Interface Anal*. **1992**, *18*, 685.
(59) Centi, G.; Pinelli, D.; Trifiro, F.; Ghoussoub, D.; Guelton, M.; Gengembre, L. *J. Catal*. **1991**, *130*, 238.
(60) Reddy, B. M.; Lakshmanan, P.; Khan, A. *J. Phys. Chem. B* **2004**, *108*, 16855.
(61) Bensalem, A.; Verduraz, F. B.; Delamar, M.; Bugli, G. *Appl.Catal., A* **1995**, *121*, 81.
(62) Burroughs, A.; Hamnett, A.; Orchard, A. F.; Thornton, G. *J. Chem. Soc., Dalton Trans*. **1976**, *1*, 1686.
(63) Noronha, F. B.; Fendley, E. C.; Soares, R. R.; Alvarez, W. E.; Resasco, D. E. *Chem. Eng. J*. **2001**, *82*, 21 and references therein.
(64) Adams, C. R.; Jennings, T. J. *J. Catal*. **1970**, *17*, 157.
(65) Shiju, N. R.; Anilkumar, M.; Mirajkar, S. P.; Gopinath, C. S.; Rao, B. S.; Satyanarayana, C. V. *J. Catal*. **2005**, *230*, 484 and references therein.
(66) Roh, H. S.; Potdar, H. S.; Jun, K. W. *Catal. Today* **2004**, *93*, 39.
(67) Xu, S.; Wang, X. *Fuel* **2005**, *84*, 563.
(68) Larrondo, S.; Vidal, M. A.; Irigoyen, B.; Craievich, A. F.; Lamas, D. G.; Abregas, I. O.; Noem, E. L.; Reca, W. D.; Amadeo, N. *Catal. Today* **2005**, *107*, 53.